ORGANOMETALLICS
Article
pubs.acs.org/Organometallics

Investigation of Ketone C═O Bond Activation Processes by Heterobimetallic Zr/Co and Ti/Co Tris(phosphinoamide) Complexes

Hongtu Zhang,[‡] Bing Wu,[‡] Seth L. Marquard, Elishua D. Litle, Diane A. Dickie, Mark W. Bezpalko, Bruce M. Foxman, and Christine M. Thomas*

Department of Chemistry, Brandeis University, 415 South Street, Waltham, Massachusetts 02454, United States

S Supporting Information

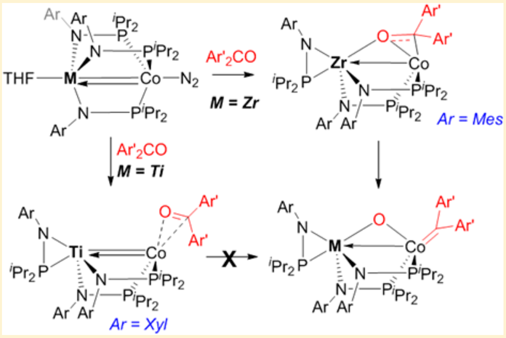

ABSTRACT: The reactivity of the reduced Zr/Co and Ti/Co complexes $\mathrm{(THF)Zr(MesNP^{i}Pr_2)_3CoN_2}$ (**1**, Mes = 2,4,6-trimethylphenyl) and $\mathrm{(THF)Ti(XylNP^{i}Pr_2)_3CoN_2}$ (**7**, Xyl = 3,5-dimethylphenyl) toward diaryl ketones is explored in an effort to gain mechanistic insight into C═O bond cleavage processes. Complex **1** reacts with 4,4′-dimethoxybenzophenone to generate $\mathrm{((\mathit{p}\text{-}OMeC_6H_4)_2CO)Zr(MesNP^{i}Pr_2)_3CoN_2}$ (**2**), which exists as a mixture of valence tautomers in solution that interconvert via electron transfer from $\mathrm{Co^{-I}}$ to the Zr-bound ketone in $\mathbf{2}^{\mathrm{S}}$ to form a Zr-bound ketyl radical in $\mathbf{2}^{\mathrm{T}}$. The geometry of **2** in the solid state is most consistent with the singlet ketone adduct tautomer $\mathbf{2}^{\mathrm{S}}$. Upon removal of the Co-bound N_2 under vacuum, complex **2** cleanly coverts to the μ-oxo carbene product $\mathrm{(\eta^2\text{-}MesNP^{i}Pr_2)Zr(MesNP^{i}Pr_2)_2(\mu\text{-}O)Co{=}C(C_6H_4\mathit{p}\text{-}OMe)_2}$ (**5**) at room temperature in solution. A diamagnetic intermediate, tentatively assigned as ketone-bridged species $\mathrm{(\eta^2\text{-}MesNP^{i}Pr_2)Zr(MesNP^{i}Pr_2)_2Co(\mu_2,\eta^1\eta^2\text{-}OC(\mathit{p}\text{-}OMeC_6H_4)_2)}$ (**6**), is observed spectroscopically during the transformation of **1** to **5**. Similar reactions between the Ti/Co analogue **7** and diaryl ketones reveal no evidence for electron-transfer to form triplet ketyl radical species. Complex **7** reacts with 4,4′-dimethoxybenzophenone to afford diamagnetic $\mathrm{((\mathit{p}\text{-}OMeC_6H_4)_2CO)Ti(XylNP^{i}Pr_2)_3CoN_2}$ (**8**). In contrast, addition of benzophenone to **7** under N_2 generates a mixture of $\mathrm{(\eta^2\text{-}XylNP^{i}Pr_2)Ti(XylNP^{i}Pr_2)_2Co(\eta^2\text{-}OCPh_2)}$ (**9**) and $\mathrm{(Ph_2CO)Ti(XylNP^{i}Pr_2)_3CoN_2}$ (**10**) in solution, and C_3-symmetric **10** is found to be favored in the solid state. Complex **9** can be generated exclusively and isolated in the absence of N_2. Ti/Co complexes **8**−**10** are thermally stable and do not undergo C═O bond cleavage even at elevated temperature, in stark contrast to their Zr/Co congeners.

INTRODUCTION

Early/late heterobimetallic complexes have been studied for a number of years, under the pretense that the inherent differences in Lewis acidity between the two metals, and in some cases, polar metal−metal bonds would lead to unique bond activation processes and reactivity patterns.[1] Early work in this area by Bergman and Wolczanski demonstrated that early/late heterobimetallic complexes could facilitate reactions including alkene reduction,[2] CO_2 and CO reduction,[3] and X−H bond activation (X = O, S, and N).[4] In more recent years, researchers such as Nagashima and Michaelis have demonstrated that early/late metal−metal interactions can enhance electrophilicity and promote allylic amination[5] and enyne cycloisomerization reactions.[6] In all cases, achieving an understanding of the role that each metal plays is pivotal for the design of new bimetallic catalysts and their applications. Herein, we explore the utility of early/late heterobimetallic complexes in the activation of the polar C═O bonds in diaryl ketones.

The cleavage of C═O double bonds has a variety of applications, both in the energy sector and organic synthesis. In the context of organic synthesis, the reductive coupling of ketones to olefins is known as the McMurry reaction. It typically involves titanium compounds and stoichiometric reducing agents, and both ketyl radical and carbenoid intermediates have been proposed.[7] C═O bond cleavage is also an important step in Fischer−Tropsch synthesis, where surface-bound metal−carbene species have also been proposed.[8] Heterobimetallic approaches to C═O bond activation present a particularly promising opportunity, as the incorporation of two metal coordination sites with varying Lewis acid/base properties facilitates binding and activation of the polar C═O bond. Indeed, heterogeneous bimetallic catalysts have shown promise for cleaving the C−O bonds involved in biomass upgrading reactions, although the origin of the "synergy" between the two metals in these systems remains poorly understood.[9]

In our studies of tris(phosphinoamide)-linked heterobimetallic complexes,[1c,10] our group has recently found that early/late heterobimetallic complexes with metal−metal multiple bonds, such as $\mathrm{(THF)Zr(MesNP^{i}Pr_2)_3CoN_2}$ (**1**, Mes = 2,4,6-trimethylphenyl) are uniquely capable of activating C═O bonds in a cooperative fashion that takes advantage of the

Received: June 13, 2017

polarity of the metal−metal bond. For example, complex **1** reacts readily with CO_2 to cleave a C═O bond and generate the μ-oxo carbonyl complex, (η^2-MesNP^{i}Pr$_2$)Zr(MesNP^{i}Pr$_2$)$_2$(μ-O)CoCO.[11] A similar, albeit more sluggish, reaction is observed between **1** and benzophenone, affording the μ-oxo carbene complex (η^2-MesNP^{i}Pr$_2$)Zr(MesNP^{i}Pr$_2$)$_2$(μ-O)Co═CPh$_2$ (**A**) upon thermolysis (Scheme 1).[12] In the latter case, ketone binding to Zr is observed prior to C═O bond cleavage, in some cases accompanied by electron transfer to generate Zr-bound ketyl radical products (**B** or **C**) rather than formation of simple ketone adducts (**D**).[13] In a related bimetallic Ti/Co bis(phosphinoamide) system, aryl ketone addition to ClTi(XylNP^{i}Pr$_2$)$_2$CoPMe$_3$ (Xyl = 3,5-dimethylphenyl) was found to lead to reductive C═O cleavage to form the corresponding alkene products, although in this case the intermediates could not be isolated or identified spectroscopically.[14]

Scheme 1

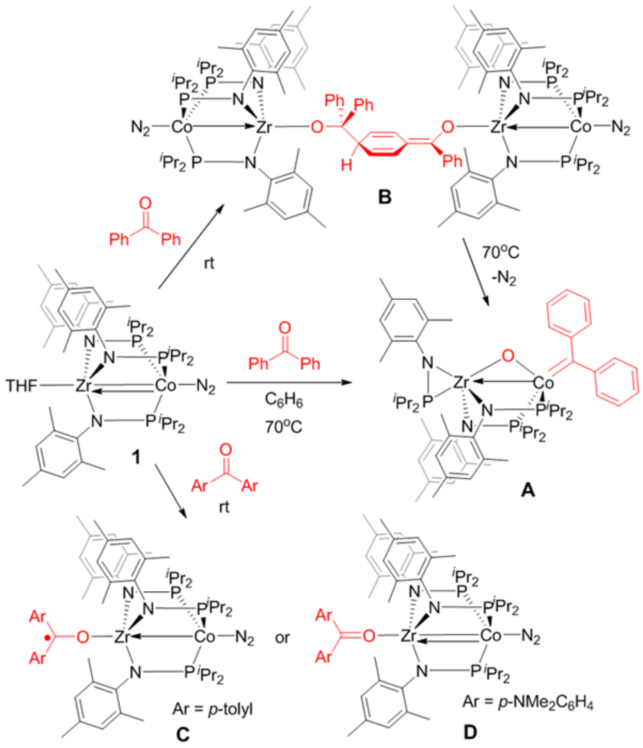

Given the similarity between the C═O bond activation reactions of CO_2 and Ar$_2$C═O facilitated by the heterobimetallic Co/Zr complex **1**, we hypothesized that similar mechanisms for these reactions could be operative. It remains unclear whether initial CO_2 coordination occurs at Zr or whether inner-sphere electron-transfer to CO_2 is an integral part of the C═O bond cleavage process. However, because ketone C═O bond cleavage is much slower than the reaction with CO_2, identifying intermediates in the ketone C═O activation process could lead to valuable insight into the CO_2 activation mechanism. A better understanding of the C═O activation process will shed light on the role that each metal plays in this cooperative bond activation process and suggest how the metal−metal combination should be tuned to better facilitate these types of bond activation reactions.

Herein, a *para*-methoxy-substituted benzophenone derivative is used to investigate the mechanism of C═O bond cleavage by a heterobimetallic Zr/Co complex. The incorporation of methoxy substituents in the para position was not only meant to prevent radical coupling processes but also was found to lead to valence tautomerism between a singlet ketone adduct and a triplet ketyl radical species. This mixture proceeds cleanly to the desired μ-oxo carbene complex in the absence of N_2, and monitoring this reaction spectroscopically allows the identification of an intermediate. Similar reactivity with heterobimetallic Ti/Co complexes is explored, revealing this metal−metal combination to be far less reactive yet allowing the isolation of analogues of the intermediate in the Zr/Co-mediated C═O bond cleavage process.

■ RESULTS AND DISCUSSION

Reactivity of 1 with 4,4′-Dimethoxybenzophenone. The initial product of benzophenone addition to **1** is the isobenzopinacol-bridged complex, **B**, shown in Scheme 1, which arises from intermolecular radical coupling of two Zr-bound ketyl radicals.[15] Monomeric ketyl radical complexes such as ((*p*-tolyl)$_2$C$^\bullet$O)Zr(MesNP^{i}Pr$_2$)$_3$CoN$_2$ (Scheme 1, **C**) can be isolated when the diaryl ketone is substituted in the para position. However, para substitution with strongly electron-donating groups such as NMe$_2$ renders the ketone sufficiently electron-rich to disfavor electron-transfer, resulting in diamagnetic ketone adducts such as ((*p*-NMe$_2$C$_6$H$_4$)$_2$C═O)Zr(MesNP^{i}Pr$_2$)$_3$CoN$_2$ (**D**).[13] Perhaps not surprisingly, a linear correlation between the Hammett parameter of the para substituent and the computed difference in energy between the singlet ketone adduct and triplet ketyl radical was observed.

Herein, we chose to explore the reactivity of **1** with 4,4′-dimethoxybenzophenone, for which the difference in energy between the $S = 0$ ketone adduct and the $S = 1$ ketyl radical is predicted to be negligible (0.3 kcal/mol) using density functional theory (DFT). The computed small difference between the singlet and triplet forms led us to anticipate that an equilibrium mixture of the two products would be generated in the reaction between 4,4′-dimethoxybenzophenone and complex **1**. Treatment of **1** with 4,4′-dimethoxybenzophenone immediately generates a new purple complex, **2** (Scheme 2). Similar to complex **1**, the cobalt-bound N_2 ligand in **2** is sufficiently labile that it can be removed *in vacuo*, as evident by a distinct reversible color change upon exposure to vacuum/N_2; however, further characterization of the N_2 free version of **2** was not pursued owing to its instability at room temperature (*vide infra*).

The room-temperature ^{1}H NMR spectrum of **2** features six relatively well-resolved resonances within the typical 0−10 ppm window expected for a diamagnetic compound, which initially led us to believe that complex **2** was simply the diamagnetic ketone adduct ((*p*-OMeC$_6$H$_4$)$_2$C═O)Zr(MesNP^{i}Pr$_2$)$_3$CoN$_2$ (**2^S**). However, upon closer inspection of the ^{1}H NMR spectrum, it became clear that the expected number of peaks was not observed and those present were shifted, broad, and lacked coupling information. Complex **2** is also ^{31}P{^{1}H} NMR silent at room temperature, inconsistent with a diamagnetic complex. Moreover, a solution magnetic moment of 1.74 μ_B was measured for **2** in C_6D_6 at room temperature. This μ_{eff} value not only is lower than the expected spin-only value for an $S = 1$ complex (2.83 μ_B) but also indicates that complex **2** is not rigorously diamagnetic.

It was hypothesized that the new purple complex, **2**, actually exists as a mixture of valence tautomers, specifically, an $S = 0$ Co^{-I} ketone adduct (**2^S**) and an $S = 1$ Co^0 ketyl radical complex

Scheme 2

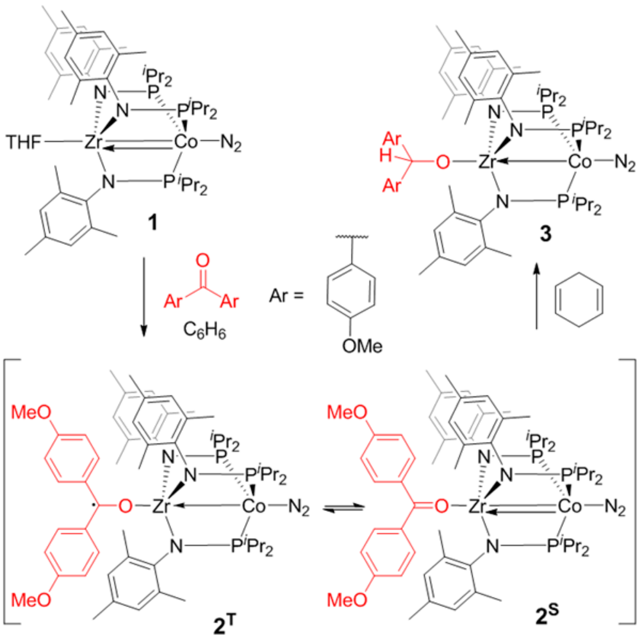

((*p*-OMeC$_6$H$_4$)$_2$C$^•$O)Zr(MesNP^{i}Pr$_2$)$_3$CoN$_2$ (**2**^{T}) in solution, related by an intramolecular one-electron transfer from Co to the Zr-bound ketone. ^{1}H NMR spectra of **2** were collected over a range of low temperatures in toluene-d_8 (25 to −45 °C, Figures S3 and S4). At 15 °C, several new paramagnetically shifted resonances begin to appear, and by −15 °C, six new peaks appear outside of the 0−8 ppm window. This behavior could be justified in several ways, but it certainly suggests that electron-transfer from Co to the Zr-bound ketone to convert **2**^{S} to **2**^{T} is rapid at room temperature. We favor the explanation that **2**^{S} and **2**^{T} are in the fast exchange limit at all temperatures and that a decrease in the fraction of **2**^{T} at low temperature is responsible for the sharper and more well-resolved paramagnetic ^{1}H NMR signals. In line with this hypothesis, a broad ^{31}P{^{1}H} NMR signal is observed at 42 ppm upon cooling a solution of **2** below 0 °C, and a decreased solution magnetic moment (μ_{eff} = 1.3 μ_B) was measured at −45 °C, supporting the idea that **2**^{S} is favored at low temperature. Taken together, it is clear that the difference in energy between **2**^{S} and **2**^{T} is very small, consistent with DFT predictions.[16] Similar to previously characterized Zr-bound ketyl radical complexes, DFT calculations of **2**^{T} reveal distribution of one unpaired electron onto the carbonyl carbon and throughout the aromatic π system of the diaryl ketone (Figure S39). Although the signals for **2**^{S} and **2**^{T} cannot be resolved by ^{1}H NMR spectroscopy at room temperature, the faster time scale of IR spectroscopy permits the observation of independent ν(N$_2$) stretches for both valence tautomers (**2**^{S}: 2023 cm^{-1}; **2**^{T}: 2045 cm^{-1}) at room temperature, with a higher intensity signal for the stretch attributed to **2**^{S} (Figure S6). The ν(N$_2$) for **2**^{S} is similar to that of Zr^{IV}Co^{-I} precursor **1** (2026 cm^{-1}),[17] and the ν(N$_2$) stretch for **2**^{T} compares well with that of other Zr^{IV}Co^0 complexes such as **C** (2045 cm^{-1})[13] or ROZr(MesNP^{i}Pr$_2$)$_3$CoN$_2$ (2041−2052 cm^{-1}).[18] A similar phenomenon was observed for the spin crossover compound [Fe(btr)$_2$(NCS)$_2$]·H$_2$O (btr = 4,4′-bis-1,2,4-triazole), in that two distinct ν(CN) stretching vibrations could be observed at temperatures in the middle of the spin transition and their ratio at different temperatures followed the same hysteresis pattern as the magnetic susceptibility measurements.[19]

The singlet tautomer of **2**^{S} is also favored in the solid state, as determined via X-ray diffraction of a single crystal grown from a solution of **2**. The resulting solid state structure shown in Figure 1 reveals geometric features most consistent with an *S* = 0 ketone adduct. For example, the C−O bond distance (1.249(3) Å) is indicative of a C═O double bond, and the carbonyl carbon could be observed at 183.9 ppm in the ^{13}C{^{1}H} NMR spectrum of **1** at −30 °C, confirming little activation of the C═O bond in **2**^{S}. The short Zr−Co distance (2.4039(4) Å) is similar to that in **1** and implicates a reduced Zr^{IV}Co^{-I} oxidation state assignment with Zr−Co multiple bond character. The geometric parameters are quite different from those observed for triplet ketyl radical species such as (fluorenone$^•$)Zr(MesNP^{i}Pr$_2$)$_3$CoN$_2$ (C−O: 1.3265(19) Å; Zr−Co: 2.6324(3) Å; Zr−O: 2.0169(11) Å).[13] Although the initial X-ray diffraction experiments were carried out at 120 K, data collection at higher temperature led to identical geometric parameters, with no signs of elongated ellipsoids or disorder that would indicate any conversion to the ketyl radical tautomer **2**^{T} at higher temperature (248 K) in the solid state.

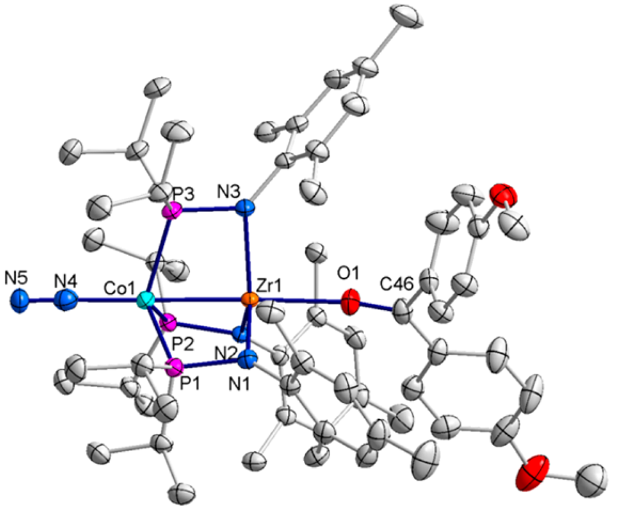

Figure 1. Displacement ellipsoid (50%) representation of **2** in the solid state. All hydrogen atoms and solvate molecules have been omitted for clarity. Selected bond distances (Å): Zr1−Co1, 2.4039(4); Zr1−O1, 2.3133(16); O1−C46, 1.249(3).

Lastly, the existence of the ketyl tautomer **2**^{T} in solutions of **2** at room temperature was further confirmed by exploring its reactivity with weak C−H bonds. Similar to reported ketyl radical complexes such as **C** or (fluorenone$^•$)Zr(MesNP^{i}Pr$_2$)$_3$CoN$_2$, a solution of **2** in 1,4-cyclohexadiene cleanly converts to the *S* = $^1/_2$ alkoxide complex ((*p*-OMeC$_6$H$_4$)$_2$CHO)Zr(MesNP^{i}Pr$_2$)$_3$CoN$_2$ (**3**) via H atom abstraction (Scheme 2).

C═O Bond Cleavage Reactions. We previously reported that thermolysis of the tetrametallic isobenzopinacol-bridged complex **B** under N$_2$ leads to both C−C and C−O bond cleavage to generate the μ-oxo carbene species (η^2-MesNP^{i}Pr$_2$)-Zr(MesNP^{i}Pr$_2$)$_2$(μ-O)Co═CPh$_2$ (Scheme 1, **A**).[12] A minor byproduct (20%) of this reaction is the μ-imido P−N bond cleavage product (Ph$_2$(^{i}Pr$_2$P)CO)Zr(μ-NMes)-(MesNP^{i}Pr$_2$)$_2$Co, and it was found that this undesired P−N cleavage pathway could be circumvented by thermolyzing **B** in the absence of N_2. A similar reaction profile was expected for complex **2**, simplified by its monomeric nature and the absence of a requisite C−C bond cleavage step. Indeed, **2** was found to undergo further reactions readily even at room temperature.

When stored at room temperature in solution under N_2 for 18 h, complex **2** transforms cleanly to a new paramagnetic complex, identified as the *μ*-imido P−N bond cleavage product (p-OMeC$_6$H$_4$)$_2$(^{i}Pr$_2$P)CO)Zr(*μ*-NMes)(MesNP^{i}Pr$_2$)$_2$Co (**4**) by comparison of its ^{1}H NMR spectrum to that reported for the benzophenone analogue (Scheme 3 and Figure S9).[12] In contrast, a thoroughly degassed solution of **2** cleanly converts to the desired *μ*-oxo carbene species (η^2-MesNP^{i}Pr$_2$)Zr(MesNP^{i}Pr$_2$)$_2$(*μ*-O)Co═C(C$_6$H$_4$$p$-OMe)$_2$ (**5**) via C═O bond cleavage over 17 h at room temperature (Scheme 3). Similar to its benzophenone-derived analogue, complex **5** adopts an $S = 1$ ground state ($\mu_{\text{eff}} = 2.87\ \mu_B$) with a large number of broad paramagnetically shifted resonances in its ^{1}H NMR spectrum owing to its asymmetric nature. Interestingly, complex **5** is also formed in ∼50% conversion when a solution of **A** is treated with stoichiometric 4,4′-dimethoxybenzophenone (Figure S12), with the concomitant appearance of free benzophenone.

Scheme 3

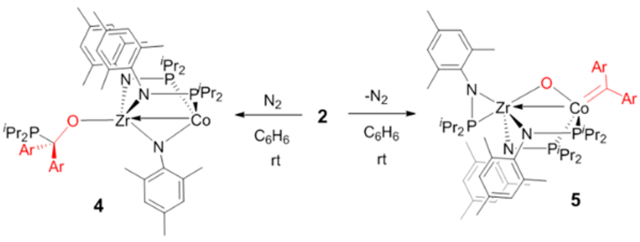

The solid state structure of **5** was determined crystallographically and is shown in Figure 2. The bond distances and angles in **5** are largely similar to its benzophenone-derived analogue **A**,[12] with slightly shorter Co−C (1.885(2) Å vs 1.906(2) Å) and longer Co−O (2.0098(16) Å vs 1.9710(16) Å) distances for **5** that may be the result of the more electron-donating aryl substituents.

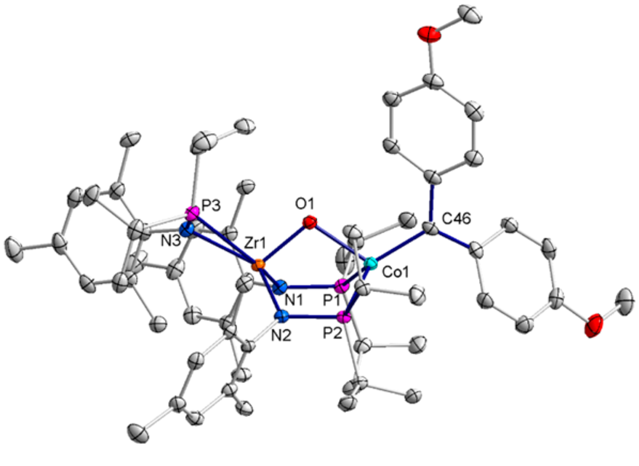

Figure 2. Displacement ellipsoid (50%) representation of **5** in the solid state. All hydrogen atoms and solvate molecules have been omitted for clarity. Selected bond distances (Å): Co1−C46, 1.885(2); Zr1−O1, 1.8291(16); Co1−O1, 2.0098(16); Co1−Zr1, 3.0594(4).

To further explore the conversion of **2** to **5** and the role that N_2 plays in the product distribution, a reaction between the N_2-free precursor (THF)Zr(MesNP^{i}Pr$_2$)$_3$Co and 4,4′-dimethoxybenzophenone was monitored at low temperature by NMR spectroscopy. Upon warming the mixture to 0 °C, a diamagnetic intermediate was observed prior to formation of **5** (Figures S11 and S12). The ^{1}H NMR resonances of the intermediate appear in the typical 0−10 ppm region, but many of the resonances were broad at 0 °C, suggesting fluxionality on the NMR time scale. The most diagnostic spectroscopic features were three peaks of identical size in the 6.3−6.7 ppm region of the spectrum, indicative of at least two inequivalent *N*-mesityl groups. These resonances can be attributed to the two aromatic protons of one phosphinoamide ligand bound terminally to Zr and two phosphinoamide ligands bridging between Zr and Co, with hindered rotation about the N−C bond resulting in two additional peaks each integrating to 2 protons. The remaining peaks in the ^{1}H NMR spectrum are broad and ill-defined, but the number of resonances observed in the aromatic region is consistent with an asymmetric product. The ^{31}P{^{1}H} NMR spectrum is more perplexing, with just a single sharp resonance at 17.2 ppm observed for the intermediate (Figure S14). Given this spectroscopic data, we tentatively assign this intermediate as (η^2-MesNP^{i}Pr$_2$)Zr(MesNP^{i}Pr$_2$)$_2$Co(μ_2,$\eta^1\eta^2$-OC(p-OMeC$_6$H$_4$)$_2$) (**6**), an N_2-free isomer of **2** in which the diaryl ketone adopts a bridging position between Zr and Co in place of one of the phosphine donors (Scheme 4). This type of intermediate is similar to the previously described product of thiobenzophenone and **1**, (η^2-MesNP^{i}Pr$_2$)Zr(MesNP^{i}Pr$_2$)$_2$Co(μ_2,$\eta^1\eta^2$-SCPh$_2$), which has a ^{31}P{^{1}H}] NMR resonance corresponding to the Zr-bound η^2-MesNP^{i}Pr$_2$ ligand at 15.9 ppm.[13] We hypothesize that the same fluxional process that broadens the ^{1}H NMR data of **6** is responsible for coalescence of the Co-bound phosphine signals in the ^{31}P{^{1}H} NMR spectrum, although decoalescence was not observed through a range of temperatures from −35 °C to room temperature.

Scheme 4

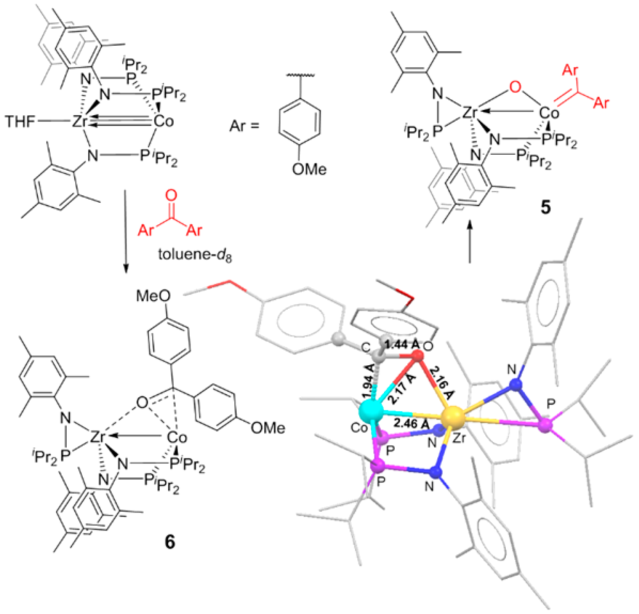

Since the proposed identity of complex **6** is quite speculative given its broad spectroscopic features and our inability to isolate this species for structural characterization, its structure was further explored computationally. Both the singlet ($\mathbf{6}^{S}$) and triplet ($\mathbf{6}^{T}$) states were calculated, and $\mathbf{6}^{S}$ was predicted to be lower in energy by 8.2 kcal/mol. The optimized geometry of intermediate $\mathbf{6}^{S}$ (Scheme 4) reveals that the diaryl ketone bridges the Co and Zr centers in a $\mu_2\eta^1\eta^2$ binding mode, with the ketone oxygen atom nearly equidistant between the Co and Zr centers. The ketone then binds η^2 to Co, with a short Co−C distance and an elongated C−O bond (1.44 vs 1.29 Å in the calculated structure of $\mathbf{2}^{S}$). The orientation of the ketone C−O bond is not perfectly parallel with the Co−Zr bond vector, disrupting the potential C_s symmetry of **6**, and the flexibility of the ketone's orientation potentially provides an explanation for some of the fluxionality of intermediate **6** observed spectroscopically in solution. On the basis of the geometry calculated for intermediate **6**, relatively little intramolecular structural reorganization is required to cleave the C−O bond and generate **5**, although the singlet-to-triplet spin transition likely contributes to the energy barrier between **6** and **5**. More comprehensive computational mechanistic studies are outside the scope of this manuscript.

Comparative Reactivity of Ti/Co Complexes with Diaryl Ketones. With information about the Zr/Co-promoted C═O bond activation process in hand, we chose to explore whether a similar ketone C═O bond cleavage process would occur when starting with the Ti/Co tris(phosphinoamide) analogue (THF)Ti(XylNP^{i}Pr$_2$)$_3$CoN$_2$ (**7**). Treatment of **7** with 4,4′-dimethoxybenzophenone affords the red-brown ketone adduct ((*p*-OMeC$_6$H$_4$)$_2$CO)Ti(XylNP^{i}Pr$_2$)$_3$CoN$_2$ (**8**, Scheme 5). The ^{31}P{^{1}H} NMR spectrum of complex **8** features a singlet at 43.4 ppm, and the ^{1}H NMR spectrum is typical of a C_3-symmetric diamagnetic complex. The IR spectrum of **8** has a sharp $\nu(N_2)$ stretch at 2067 cm^{-1}, which is 17 cm^{-1} lower in energy than the $\nu(N_2)$ of precursor **7** (2084 cm^{-1}).[20] The increased π-backbonding in ketone adduct **8** is indicative of a more electron-rich Co center, which suggests that Co → Ti donation is weakened upon replacement of THF with a diaryl ketone at the Ti coordination site *trans* to Co.

Scheme 5

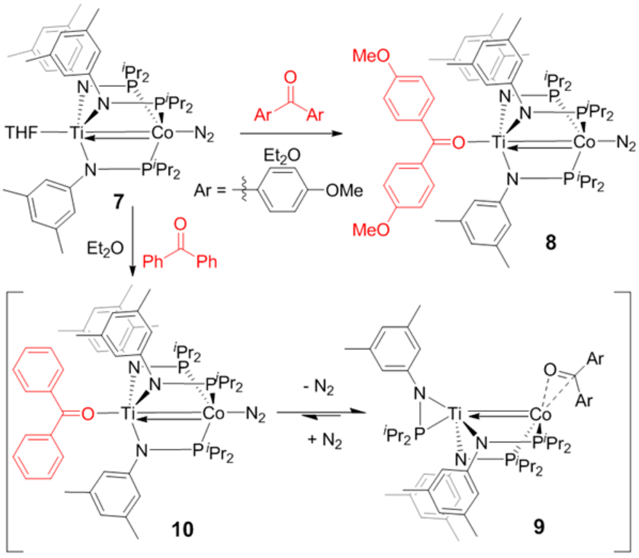

The solid-state structure of **8** was determined using single crystal X-ray diffraction (Figure 3). Similar to the solid-state structure of **2**, the bond metrics are indicative of a singlet ketone adduct. For example, the C−O bond distance (1.242(3) Å) is indicative of a C═O double bond, and this is in line with the observed downfield ^{13}C{^{1}H} NMR chemical shift for the carbonyl carbon at 199.3 ppm. The Ti−Co distance (2.2524(5) Å) is similar to that in precursor **7** (2.2371(3) and 2.22685(3) Å in two independent molecules in the asymmetric unit),[20] indicating that Ti/Co multiple bonding remains intact. In fact, the slightly elongated Ti−Co distance in **8** is consistent with a weaker Co → Ti interaction, as also concluded by the lower frequency $\nu(N_2)$ stretch.

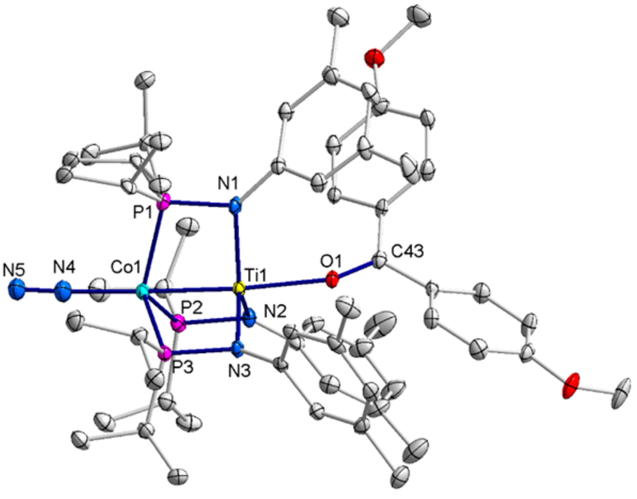

Figure 3. Displacement ellipsoid (50%) representation of **8** in the solid state. All hydrogen atoms and solvate molecules have been omitted for clarity. Selected bond distances (Å): Ti1−Co1, 2.2524(5); Ti1−O1, 2.1690(17); O1−C43, 1.242(3).

Prolonged exposure of **8** to vacuum resulted in decomposition to an intractable mixture of products, suggesting that **8** is unstable in the absence of N$_2$. However, thermolysis of **8** at 80 °C under N$_2$ for several hours resulted in no spectroscopic changes, in stark contrast to its Zr/Co analogue.

Anticipating that electron transfer to form a Ti-bound ketyl radical would be more likely with a less electron-rich diaryl ketone, the reactivity of **7** was also explored with benzophenone. Addition of benzophenone to **7** under N$_2$ affords a mixture of two diamagnetic products in solution (Scheme 5). The major product has three broad ^{31}P{^{1}H} NMR resonances at 44.1, 35.5, and 1.6 ppm in a 1:1:1 integral ratio, indicative of a product, (η^2-XylNP^{i}Pr$_2$)Ti(XylNP^{i}Pr$_2$)$_2$Co(η^2-OCPh$_2$) (**9**), with one phosphinoamide ligand dissociated from Co and bound to Ti in an η^2 fashion. The inequivalence of the two Co-bound phosphines suggests that the ketone binds in a manner that further breaks the symmetry of the molecule. An additional broad ^{31}P{^{1}H} resonance at 45.9 ppm is observed, and the similarity of the chemical shift to that of **8** suggests that the C_3-symmetric N$_2$-bound species (Ph$_2$CO)Ti(XylNP^{i}Pr$_2$)$_3$CoN$_2$ (**10**) is also present as a minor product in solution. The presence of **10** was confirmed by the appearance of a $\nu(N_2)$ stretch at 2070 cm^{-1} in the IR spectrum of the reaction mixture.

Variable-temperature NMR studies under N$_2$ reveal sharpening of the ^{31}P{^{1}H} resonances corresponding to **9** at temperatures below 15 °C (Figure S26). The broad singlet corresponding to **10** sharpens and increases in integration with respect to the signals for **9** as the temperature decreases to −35 °C. At higher temperatures, the $^{31}P\{^1H\}$ resonances for **9** and **10** coalesce into a single broad singlet centered at 44 ppm at 75 °C. The ^1H NMR spectra collected in the −35 to 75 °C temperature range generally follow the same pattern, with a lower coalescence temperature owing to the faster time scale of ^1H NMR compared to $^{31}P\{^1H\}$ NMR spectroscopy (Figure S27). Taken together, these data indicate that **9** and **10** are in equilibrium in solution under N_2, with **10** favored at lower temperatures. At room temperature an equilibrium constant (K_{eq}) of 2.5 can be estimated for **10** $\leftrightharpoons$ **9**, and the variable-temperature $^{31}P\{^1H\}$ NMR data can be used to construct a Van 't Hoff plot that provides an estimate of ΔH (1.1 kcal/mol) and ΔS (5.5 e.u., Figure S29).[21] Attempts were made to fit the dynamic variable temperature $^{31}P\{^1H\}$ NMR data to obtain exchange rates and calculated activation energies via Eyring analysis, but the only conclusion that could be drawn was that the interconversion of **9** and **10** is a complicated multistep equilibrium, and this data is included in Figures S30−S32 for the interested reader. X-ray diffraction of single crystals grown from the equilibrium mixture of **9** and **10** under N_2 reveal that the C_3-symmetric N_2-bound ketone adduct **10** is favored in the solid state, with a geometry similar to the *para*-methoxy substituted analogue **8** (Figure S38).

The asymmetric product **9** can, however, be isolated when the reaction between **7** and benzophenone is performed under argon instead of N_2. X-ray diffraction of single crystals of **9** affords the solid state structure shown in Figure 4. Consistent with the asymmetry observed by $^{31}P\{^1H\}$ NMR spectroscopy, complex **9** has one phosphinoamide ligand dissociated from Co and bound η^2 to Ti, while the remaining Co-bound phosphines are rendered inequivalent by the side-on η^2 binding of the benzophenone C═O moiety to Co. The Co−C (2.072(2) Å) and Co−O (1.8535(14) Å) distances reveal that Co is tightly bound to both atoms, and the C−O distance (1.336(2) Å) is elongated and indicative of significant activation of the C═O bond. In fact, the $^{13}C\{^1H\}$ NMR chemical shift of the ketone carbon in complex **9** is 89.3 ppm, which is shifted upfield by 100 ppm compared to the $^{13}C\{^1H\}$ resonance for the C═O functionality of **8**. While examples of late metal η^2-diarylketone adducts are limited to Ni complexes for which the $OCPh_2$ $^{13}C\{^1H\}$ resonance was not reported,[22] the $^{13}C\{^1H\}$ NMR chemical shift and the C−O bond distance in **9** are similar to those reported for early metal (Nb, Ti, and Zr) η^2-benzophenone complexes.[23] The Ti center in **9** is not involved in any interactions with the ketone (Ti−O1 interatomic distance >3.5 Å), which is quite unexpected given the oxophilicity of titanium.

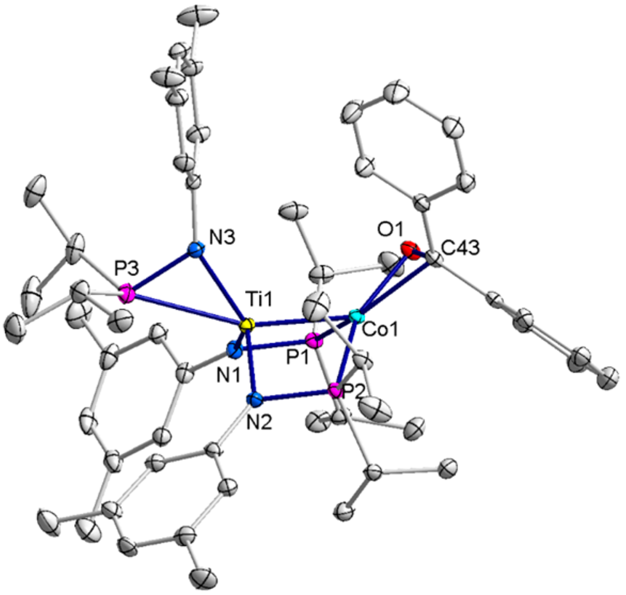

Figure 4. Displacement ellipsoid (50%) representation of **9** in the solid state. All hydrogen atoms have been omitted for clarity. Selected bond distances (Å): Co1−O1, 1.8535(14); Co1−C43, 2.072(2); Ti1−Co1, 2.2627(5); O1−C43, 1.336(2).

The spectroscopic properties of **9** are similar to those of **6**, the intermediate observed during C═O bond cleavage in the Zr/Co case (*vide supra*). However, the largest structural difference between **9** and the calculated structure of **6** is the clear absence of a Ti−O interaction in **9**. The geometry of **9** is well-replicated using the same DFT computational methods, suggesting the difference in ketone binding mode between **6** and **9** is not simply an artifact of comparing experimental and computational data. A calculation of **9** starting from a geometry more similar to **6** affords an optimized geometry of another isomer, **9′**, with the ketone bound in a $\mu_2\eta^1\eta^2$ fashion to Ti and Co. However, **9′** is found to be 18.8 kcal/mol higher in energy than **9**. Similarly, a geometric isomer of **6** with the ketone bound to Co in an η^2 fashion, **6′**, can also be computed by starting the geometry optimization at a geometry closer to that of **9**. In this case, **6′** is 12.9 kcal/mol higher in energy than **6**^{S}, demonstrating that the proposed and observed geometries of **6** and **9**, respectively, are indeed computationally predicted to differ in spatial arrangement of the bound ketone.

Thermolysis of either the mixture of **9** and **10** under N_2 or complex **9** under argon at 80 °C does not lead to any spectroscopic changes, again indicating that C═O bond cleavage is much less favorable for Ti/Co complexes compared to their Zr/Co analogues. This difference between the Zr/Co and Ti/Co systems likely relates to the aforementioned differences in ketone binding mode in intermediates **6** and **9**, which suggests that the Ti center is less Lewis acidic than the Zr center and that the oxophilicity of the group IV metal is the key driving force for C═O bond cleavage. Such a large difference in inherent electrophilicity between Ti and Zr is unexpected but may be related to differences in interactions of the early metals with Co in species such as **6** and **9**. Comparison of metal−metal distances in species containing metals of different sizes is facilitated by using Cotton's formal shortness ratio (FSR),[24] which is the ratio of the metal−metal distance to the sum of the single bond atomic radii (Pauling's R_1)[25] of the two atoms. The Ti−Co distance in complex **9** corresponds to an FSR of 0.91, indicating that substantial metal−metal multiple bonding is still present. The calculated Zr−Co distance in **6** (2.46 Å), corresponds to a slightly larger FSR (0.94), and the weaker metal−metal interaction in **6** may be correlated with its enhanced reactivity toward C═O activation.

The reluctance of Ti/Co tris(phosphinoamide) complexes to cleave ketone C═O bonds also lies in stark contrast to a previously reported Ti/Co bis(phosphinoamide) complex, $ClTi(XylNP^iPr_2)_2CoPMe_3$, that was shown to reductively couple ketones to alkenes readily at room temperature (McMurry coupling).[14] A straightforward explanation for the enhanced reactivity of the bis(phosphinoamide) Ti/Co complex can also be reached by invoking Lewis acidity arguments: With only two amide ligands, the Ti center in the bis(phosphinoamide) complex is more electrophilic/oxophilic than that in the tris(phosphinoamide) case, rendering the bis(phosphinoamide) Ti/Co complex more reactive toward C═O bond cleavage than its tris(phosphinoamide) analogue.

It is also worth highlighting another key difference between the Ti/Co and Zr/Co systems. In the Ti/Co case, there is no evidence for electron transfer from Co to form a Ti-bound ketyl radical in either solution or the solid state, while the Zr/Co complexes effectively reduce all but the most electron-rich diaryl ketones.[13,15] While a direct comparison of the redox potentials of **1** and **7** would be enlightening, we have thus far been unable to make this comparison owing to the electrochemical irreversibility of the oxidation processes and the reactivity of the resulting species with most common electrolytes and polar solvents. However, information about the reducing nature of the Co centers in **1** and **7** can be indirectly gleaned through the comparison of the degree of π-backbonding to N_2 as measured by $\nu(N_2)$ stretches. The $\nu(N_2)$ of Zr/Co complex **1** is 2026 cm^{-1}, indicating a Co center much more electron-rich than that in Ti/Co complex **7** (2084 cm^{-1}), which is consistent with the tendency for the Zr/Co complex to reduce diaryl ketones. The origin of this electronic difference between the Zr/Co and Ti/Co systems may be related to the nature of the metal−metal interactions in these complexes. Although the FSRs of **1** and **7** are identical (0.90),[17,20] the metal−metal bonding in the Ti/Co complex was found to be more covalent in nature based on the smaller difference in computed natural charge between the two metals (**1**: 1.39 (Zr)/−1.22 (Co); **7**: 0.45 (Ti)/−1.14 (Co)),[20] potentially strengthening the metal−metal interaction and decreasing the driving force for electron-transfer processes. The more positive natural charge on Zr in **1** is also consistent with its enhanced oxophilicity.

CONCLUSIONS

The reactivity of reduced heterobimetallic complexes **1** and **7**, comprised of a group IV metal (Ti and Zr) and cobalt, toward ketone has been explored to better understand the mechanism of the C═O bond cleavage process and the unique role that each metal plays. In the Zr/Co case, electron transfer to form a Zr-bound ketyl radical occurs for all but the most electron-rich diaryl ketones. 4,4′-Dimethoxybenzophenone presents a unique scenario in which the singlet ketone adduct and the triplet ketyl radical products are sufficiently similar in energy that both exist simultaneously in solution at room temperature as valence tautomers. In the absence of N_2, the initial product of ketone binding and/or reduction readily transforms into an μ-oxo cobalt carbene product via C═O bond cleavage. When this reaction is monitored at low temperature, an asymmetric diamagnetic intermediate is observed spectroscopically, and it is proposed that this intermediate is a bridging $\mu_2\eta^1\eta^2$ ketone adduct. A DFT geometry optimization of this proposed intermediate suggests that the ketone oxygen atom bridges between Zr and Co and suggests significant activation of the C═O bond.

In the case of Ti/Co analogues, ketone reduction does not occur, and this may be the result of a stronger metal−metal interaction attenuating the electron density at the Co center. In the absence of N_2, an asymmetric diamagnetic complex is isolated upon addition of 4,4′-dimethoxybenzophenone to the reduced Ti/Co complex, **7**. This product has similar spectroscopic features to the intermediate observed in the Zr/Co analogue, but its structural characterization reveals that the ketone binds exclusively to Co in an η^2 fashion, with no evidence for any interaction between Ti and the ketone oxygen atom. In the reactions of the Ti/Co complex with diaryl ketones, there is no evidence for further C═O bond cleavage reactions to generate μ-oxo carbene products, allowing us to infer that interaction of the ketone oxygen with the group IV metal is a necessary prerequisite to C═O bond cleavage. The small difference in electronegativity, and therefore oxophilicity, between Zr and Ti is sufficient to engender different reactivity. This study serves to highlight the subtle interplay between the early and late metals in these bimetallic systems.

EXPERIMENTAL SECTION

General Considerations. Unless specified otherwise, all manipulations were performed under an inert atmosphere using standard Schlenk or glovebox techniques. Glassware was oven-dried before use. Benzene, pentane, diethyl ether, tetrahydrofuran, and toluene were sparged with ultra-high-purity argon and dried via passage through drying columns using a solvent purification system from Pure Process Technologies. All solvents were stored over 3 Å molecular sieves. Benzene-d_6 and toluene-d_8 (Cambridge Isotopes) were degassed via repeated freeze−pump−thaw cycles and dried over 3 Å molecular sieves. (THF)Zr(MesNP^{i}Pr$_2$)$_3$CoN$_2$ (**1**) and (THF)Ti(XylNP^{i}Pr$_2$)$_3$CoN$_2$ (**7**) were synthesized using literature procedures.[17,20] All other chemicals were purchased from commercial vendors and used without further purification. For ^{1}H and ^{13}C NMR spectra, the solvent resonance was referenced as an internal standard, and for ^{31}P{^{1}H} NMR spectra, the 85% H_3PO_4 resonance was referenced as an external standard (0 ppm). IR spectra were recorded on a Varian 640-IR spectrometer controlled by Resolutions Pro software. UV−vis spectra were recorded on a Cary 50 UV−vis spectrophotometer using Cary WinUV software. Elemental analyses were performed by Robertson Microlit Laboratories, Ledgewood, NJ. Solution magnetic moment measurements were obtained using Evans' method.[26]

X-ray Crystallography Procedures. All operations were performed on a Bruker-Nonius Kappa Apex2 diffractometer, using graphite-monochromated Mo Kα radiation. All diffractometer manipulations, including data collection, integration, scaling, and absorption corrections were carried out using the Bruker Apex2 or Apex3 software suites.[27] Fully labeled diagrams and data collection and refinement details are included in Tables S1 and S2 and pages S24−S36. Further crystallographic details may be found in CCDC 1553733−1553737.

Computational Details. All calculations were performed using Gaussian09, revision A.02, for the Linux operating system.[28] Density functional theory calculations were carried out using a combination of Becke's 1988 gradient-corrected exchange functional[29] and Perdew's 1986 electron correlation functional[30] (BP86). A mixed-basis set was employed, using the LANL2TZ(f) triple-ζ basis set with effective core potentials for cobalt, titanium, and zirconium,[31] Gaussian09's internal 6-311+G(d) for heteroatoms (nitrogen, oxygen, and phosphorus), and Gaussian09's internal LANL2DZ basis set (equivalent to D95 V)[32] for carbon and hydrogen. The computational methods used in this study were chosen for the sake of consistency with previous studies. This functional and basis set combination has been successful in accurately predicting geometries and spin states that correlate well with experimental results in previous studies on similar heterobimetallic Zr/Co and Ti/Co complexes.[13,14,17,20,33] Using crystallographically determined geometries as a starting point and modifying as needed, the geometries were optimized to a minimum, followed by analytical frequency calculations to confirm that no imaginary frequencies were present. Further computational details are presented on pages S37−S40 of the Supporting Information.

((*p*-OMeC$_6$H$_4$)$_2$CO)Zr(MesNP^{i}Pr$_2$)$_3$Co(N$_2$) (2). Complex **1** (100 mg, 0.0969 mmol) was dissolved in diethyl ether (2 mL) at room temperature. This dark brown solution was added to solid 4,4′-

dimethoxybenzophenone (24.2 mg, 0.100 mmol), and the solution was diluted to 3 mL. The reaction mixture was allowed to stir for 20 min, then dried under vacuum. The resulting residue was triturated with pentane (4 mL) to form a dark colored solid that was collected by filtration. The solid was then extracted into diethyl ether and filtered through glass microfiber filter paper. The diethyl ether solution was concentrated and stored at −35 °C overnight, resulting in dark purple crystalline solids (83.9 mg, 72%). Crystals suitable for X-ray diffraction were grown from pentane solution at −35 °C. ^{1}H NMR (400 MHz, 298 K, C_6D_6): δ 9.41 (br), 6.87 (s), 3.00 (br s), 2.55 (s), 2.25 (s), 0.85 (br s). ^{1}H NMR (400 MHz, 258 K, C_6D_6): δ 27.9 (br), 26.7 (br), 18.4 (br), 9.0 (br), 6.87 (s), 2.90 (br), 2.49 (s), 2.20 (s), 0.98 (br s), −1.97 (br), −2.33 (br), −47.5 (br). ^{13}C{^{1}H} NMR (100.5 MHz, 243 K, toluene-d_8): (Not all expected resonances were identified, and many likely overlap with toluene residual solvent signals.) δ 183.9 (br), 153.1 (br), 138.7 (s), 137.1 (s), 131.7 (s), 130.3 (s), 129.9 (s), 122.6 (s), 80.6 (br), 65 (br), 40.9 (br), 34.8 (br). ^{31}P{^{1}H} NMR (toluene-d_8, 228 K, 162 MHz): δ 42 (br s). IR (C_6D_6): 2023 cm^{-1} (**2**^{S}-N_2), 2045 cm^{-1} (**2**^{T}-N_2), 1655 cm^{-1} (**2**^{S}-CO). UV−vis (C_6H_6, λ(nm) (ε, M^{-1} cm^{-1}): 510 (1.86×10^3), 683 (sh). Evans' method (μ_{eff}, C_6D_6): 1.74 μ_B (298 K), 1.3 μ_B (228 K). Satisfactory elemental analysis data for **2** could not be obtained owing to its thermal instability and tendency to convert to **3**, **4**, and/or **5** over time at room temperature.

((*p*-OMeC$_6$H$_4$)$_2$CHO)Zr(MesNP^{i}Pr$_2$)$_3$Co(N$_2$) (3). Complex **2** (35 mg, 0.030 mmol) was dissolved in 1,4-cyclohexadiene (0.5 mL) and stirred at room temperature for 24 h. The reaction mixture was dried *in vacuo*. The resulting solid was triturated with pentane (1 mL) to afford a yellow-green powder, which was redissolved in pentane (4 mL) and filtered through a piece of glass microfiber filter paper. The filtrate was stored at −35 °C overnight to yield a yellow crystalline solid. The supernatant was decanted and the solid product was washed with minimal pentane (31.6 mg, 90%). ^{1}H NMR (400 MHz, C_6D_6): δ 9.3, 8.02−8.00 (m), 7.52 (s), 6.97−6.95 (m), 5.8 (br), 3.6 (s), 2.7 (br), 2.2 (s), −1.7 (br). IR (C_6D_6): 2044 cm^{-1} (Co−N_2). UV−vis (C_6H_6, λ(nm) (ε, M^{-1} cm^{-1})): 608 (sh), 505 (330), 402 (3120). Evans' method (μ_{eff}, C_6D_6): 1.71 μ_B Anal. Calcd for $C_{60}H_{89}CoN_3O_3P_3Zr$: C, 63.02; H, 7.85; N, 3.67. Found: C, 59.36; H, 7.37; N, 4.08. Repeated elemental analysis results were low in %C and %N, which can be attributed to the air/moisture sensitivity of **3** and the lability of the Co-bound N_2 ligand under vacuum. Addition of three O atoms corresponding to oxidation of all three phosphines would, indeed, result in theoretical %C and %H values more consistent with the obtained elemental percentages (Anal. Calcd for $C_{60}H_{89}CoN_5O_6P_3Zr$: C, 59.10; H, 7.36; N, 5.74).

(*p*-OMeC$_6$H$_4$)$_2$(^{i}Pr$_2$P)CO)Zr(*μ*-NMes)(MesNP^{i}Pr$_2$)$_2$Co (4). Complex **2** (35 mg, 0.029 mmol) was dissolved in benzene (8 mL) in a 20 mL scintillation vial. The vial was taped and allowed to stand at room temperature for 18 h without stirring. The solution color gradually changed from dark purple to bright red. The solvent was removed *in vacuo* to obtain a yellow-orange powder. The solid was then redissolved in pentane, filtered, concentrated under vacuum, and stored at −35 °C to precipitate complex **4** as a dark solid after 48 h (14.1 mg, 41%). ^{1}H NMR (400 MHz, C_6D_6): δ 28.70, 13.80, 8.05, 7.01, 5.35, 3.58, 3.34 (br), 2.15, 2.07 (br), 1.08, 0.55, −10.25. ^{31}P{^{1}H} NMR (161.8 MHz, C_6D_6): δ 34.3. The ^{1}H NMR spectrum of **4** was very similar to that previously reported for (Ph$_2$(^{i}Pr$_2$P)CO)Zr(μ-NMes)(MesNP^{i}Pr$_2$)$_2$Co (see Figure S9), so its characterization was not pursued further.[12]

(η^2-MesNP^{i}Pr$_2$)Zr(MesNP^{i}Pr$_2$)$_2$(*μ*-O)Co═C(*p*-OMeC$_6$H$_4$)$_2$ (5). Complex **2** (60 mg, 0.051 mmol) was dissolved in benzene (3 mL) in a Schlenk tube containing a stir bar and sealed with a Teflon valve. The flask was then degassed on the Schlenk line using four freeze−pump−thaw cycles, resulting in a color change from dark purple to brown-red. The solution was allowed to stir for 17 h under argon atmosphere. The volatiles were removed under vacuum. The resulting dark brown residue was triturated with pentane (3 mL) to afford a black-brown solid. Crystalline product was obtained through pentane extraction and filtration followed by concentration and storage at −35 °C (54.3 mg, 93%). Crystals suitable for X-ray diffraction were chosen from a batch of crystals grown in this fashion. ^{1}H NMR (400 MHz, C_6D_6): δ 68.7, 55.3, 28.8, 30.9, 13.4, 10.3, 6.3, 3.3, 2.6, 2.2, 2.0, 0.6, −0.9, −1.7, −4.8, −5.4, −9.2, −10.6, −11.5. UV−vis (C_6H_6, λ(nm) (ε, M^{-1} cm^{-1}): 750 (986), 572 (1.44×10^3), 482 (1740), 352 (6470). Evans' method (μ_{eff}, C_6D_6): 2.87 μ_B. Anal. Calcd for $C_{60}H_{89}CoN_3O_3P_3Zr$: C, 63.02; H, 7.85; N, 3.67. Found: C, 59.99; H, 7.52; N, 3.46. Repeated elemental analysis results were low in %C, which can be attributed to the air/moisture sensitivity of **5**. Addition of three O atoms corresponding to oxidation of all three phosphines would, indeed, result in theoretical values more consistent with the obtained elemental percentages (Anal. Calcd for $C_{60}H_{89}CoN_3O_6P_3Zr$: C, 60.49; H, 7.53; N, 3.53).

Detection of (η^2-MesNP^{i}Pr$_2$)Zr(MesNP^{i}Pr$_2$)$_2$Co(μ_2,$\eta^1\eta^2$-OC(p-OMeC$_6$H$_4$)$_2$) Intermediate (6). The N_2-free compound (THF)Zr(MesNP^{i}Pr$_2$)$_3$Co was generated *in situ* via pulling vacuum on a toluene-d_8 solution complex of **1** (27.1 mg, 0.027 mmol) in an argon-filled glovebox. The resulting green/blue solution was cooled to −35 °C in the glovebox freezer, and to this was added a cold solution of 4,4′-dimethoxybenzophenone (6.8 mg, 0.028 mmol) in toluene-d_8 (0.5 mL). The tube was quickly removed from the glovebox and frozen in liquid nitrogen to halt reaction progress. The NMR tube was then immediately inserted into an NMR probe precooled to −35 °C. The ^{1}H and ^{31}P{^{1}H} NMR spectra were monitored as the solution was slowly warmed to room temperature. See Figure S14 for ^{31}P{^{1}H} NMR spectra monitoring the reaction progress as the temperature is increased, and see Figure S13 for the diamagnetic region of the ^{1}H NMR spectrum at 0 °C where signals for diamagnetic intermediate **6** can be detected. ^{1}H NMR (400 MHz, 273 K, toluene-d_8; many resonances are broad, ill-defined, and overlapping; only the most diagnostic peaks are listed): δ 6.90 (s, 4H), 6.69 (s, 2H), 6.55 (s, 2H), 6.43 (s, 2H), 3.34 (s), 2.41−2.62 (br m), 2.66 (s), 2.31 (s), 2.21 (s), 2.13 (s), 2.07 (s), 1.48 (br m), 1.30 (br m), 1.23 (br m), 0.86−1.02 (br m). ^{31}P{^{1}H} NMR (toluene-d_8, 283 K, 162 MHz): δ 17.2 (s, 1P), the other two ^{31}P resonances are not detected, likely owing to fluxionality.

((*p*-OMeC$_6$H$_4$)$_2$CO)Ti(XylNP^{i}Pr$_2$)$_3$CoN$_2$ (8). In a 20 mL scintillation vial, (THF)Ti(XylNP^{i}Pr$_2$)$_3$CoN$_2$ (**7**) (75 mg, 0.082 mmol) was dissolved in 2 mL of diethyl ether. To this solution was added a solution of 4,4′-dimethoxybenzophenone (20 mg, 0.082 mmol) in 2 mL of diethyl ether. After 5 min of swirling, the brown solution was concentrated *in vacuo* to approximately 2 mL. After standing at room temperature for 24 h, the mother liquor was decanted from the reddish brown crystalline material affording 55 mg of **8** (62%) as a crystalline solid. X-ray quality crystals were chosen from those grown in this manner. ^{31}P{^{1}H} NMR (C_6D_6, 298 K, 162 MHz): δ 43.4 (s). ^{1}H NMR (C_6D_6, 400 MHz): δ 6.93 (d, J_{H-H} = 8 Hz, 4H, O═C*Ar*$_2$), 6.71 (br s, 6H, *o*-Xyl), 6.48 (d, J_{H-H} = 8.4 Hz, 4H, O═C*Ar*$_2$), 6.34 (br s, 3H, *p*-Xyl), 3.34 (br m, 6H, C*H*(CH$_3$)$_2$), 3.25 (s, 6H, OMe), 2.02 (s, 18H, Xyl−Me), 1.72 (br m, 18H, CH(C*H*$_3$)$_2$), 1.54 (br m, 18H, CH(C*H*$_3$)$_2$). ^{13}C{^{1}H} NMR (C_6D_6, 100.6 MHz): δ 199.3 (*C*═O), 163.3, 152.7, 137.2, 133.4, 129.7, 124.1, 122.8, 113.0, 54.8, 35.6, 21.4, 20.7. IR (C_6D_6): 2067 cm^{-1} (N_2), 1651 cm^{-1} (CO). UV−vis (Et_2O) λ_{max}, nm (ε, L mol^{-1} cm^{-1}): 250 (15000), 295 (5800), 483 (630), 681 (110). Multiple attempts at obtaining satisfactory elemental analysis were unsuccessful owing to the instability of this compound under vacuum or in the absence of N_2.

Generation of a Mixture of (η^2-XylNP^{i}Pr$_2$)Ti(XylNP^{i}Pr$_2$)$_2$Co(η^2-OCPh$_2$) (9) and (Ph$_2$CO)Ti(XylNP^{i}Pr$_2$)$_3$CoN$_2$ (10). In a 20 mL scintillation vial, (THF)Ti(XylNP^{i}Pr$_2$)$_3$CoN$_2$ (**7**) (75 mg, 0.082 mmol) was dissolved in 2 mL of pentane. To this solution was added a solution of benzophenone (15 mg, 0.082 mmol) in 2 mL of pentane. After 5 min of stirring, the brown solution was concentrated *in vacuo* to approximately 1 mL. After standing at −35 °C for 24 h, the mother liquor was decanted from the reddish brown crystalline material affording 61 mg of **9**/**10** (72%) as a crystalline solid. X-ray quality crystals were chosen from those grown in this manner. ^{31}P{^{1}H} NMR (C_6D_6, 298 K, 162 MHz): δ 45.9 (br s, **10**), 44.1 (br s, **9**), 35.5 (br s, **9**), 1.6 (s, **9**). Owing to the relatively small proportion of **10** in the mixture, ^{1}H and ^{13}C{^{1}H} NMR signals could not be unambiguously distinguished from those of **9**. ^{1}H and ^{13}C{^{1}H} NMR spectra are included in the Supporting Information. IR of **10** (C_6D_6): 2070 cm^{-1} (N_2), 1663 (CO). Anal. Calcd for **10**,

$C_{55}H_{79}CoN_5OP_3Ti$: C, 64.39; H, 7.76; N, 6.83. Found: C, 63.65; H, 7.85; N, 5.89. Elemental analysis was consistently low on %N, likely owing to the lability of the bound N_2 in **10**. UV−vis (Et_2O) λ_{max}, nm (ε, L mol^{-1} cm^{-1}): 252 (13 000), 303 (3600), 440 (590), 688 (140).

(η^2-XylNP^{i}Pr$_2$)Ti(XylNP^{i}Pr$_2$)$_2$Co(η^2-OCPh$_2$) (9). In an argon-filled glovebox, (THF)Ti(XylNP^{i}Pr$_2$)$_3$CoN$_2$ (**7**) (75 mg, 0.082 mmol) was dissolved in 2 mL of pentane in a 20 mL scintillation vial. To this solution was added a solution of benzophenone (15 mg, 0.082 mmol) in 2 mL of pentane. After 5 min of swirling, the brown solution was concentrated *in vacuo* to approximately 1 mL. After standing at −35 °C for 24 h, the mother liquor was decanted from the reddish brown crystalline material affording 58 mg of **9** (71%) as a crystalline solid. X-ray quality crystals were chosen from those grown in this manner. $^{31}P\{^1H\}$ NMR (C_6D_6, 298 K, 162 MHz): δ 44.0 (br s), 35.3 (br s), 1.4 (s). ^1H NMR (C_6D_6, 298 K, 400 MHz): δ 7.96 (br s, 2H, O═C*Ar*$_2$), 7.36 (br s, 2H, O═C*Ar*$_2$), 7.05 (br s, 2H, O═C*Ar*$_2$), 7.00 (br s, 2H, O═C*Ar*$_2$), 6.81−6.90 (m, 6H, Xyl), 6.55−6.64 (br m, 3H, Xyl), 3.96 (br m, 1H, C*H*(CH$_3$)$_2$), 3.67 (br m, 1H, C*H*(CH$_3$)$_2$), 3.21 (br m, 1H, C*H*(CH$_3$)$_2$), 2.87 (br m, 1H, C*H*(CH$_3$)$_2$), 2.64 (br m, 3H, CH(C*H*$_3$)$_2$), 2.23 (s, 12H, Xyl−Me), 2.20 (s, 6H, Xyl−Me), 2.07 (br m, 3H, CH(C*H*$_3$)$_2$), 1.81 (br m, 1H, C*H*(CH$_3$)$_2$), 1.67 (br m, 6H, CH(C*H*$_3$)$_2$), 1.32 (br m, 3H, CH(C*H*$_3$)$_2$), 1.19 (br m, 3H, CH(C*H*$_3$)$_2$), 1.01 (br m, 3H, CH(C*H*$_3$)$_2$), 0.82 (br m, 3H, CH(C*H*$_3$)$_2$), 0.55 (br m, 9H, overlapping CH(C*H*$_3$)$_2$), 0.43 (br m, 3H, CH(C*H*$_3$)$_2$), one C*H*(CH$_3$)$_2$ proton could not be resolved due to overlap. $^{13}C\{^1H\}$ NMR (C_6D_6, 298 K, 100.6 MHz): δ 153.2, 151.6, 150.8, 146.7, 143.3, 137.7, 137.4, 136.9, 131.1, 126.9, 125.9, 125.8, 124.5, 124.1, 123.7, 123.5, 122.5, 121.1, 89.3 (*C*═O), 32.5, 31.4, 28.8, 26.8, 23.0, 22.5, 21.2, 20.3, 19.9, 19.0, 18.4, 18.0, 16.3. UV−vis (Et_2O) λ_{max}, nm (ε, L mol^{-1} cm^{-1}): 250 (15 000), 310 (4800), 650 (980). Anal. Calcd for $C_{55}H_{79}CoN_3OP_3Ti$: C, 66.19; H, 7.98; N, 4.21. Found: C, 64.65; H, 8.00; N, 4.26. Repeated elemental analysis results were low in %C, which can be attributed to the air/moisture sensitivity of **9**. Addition of one O atom corresponding to oxidation of one phosphine ligand would, indeed, result in theoretical values more consistent with the obtained elemental percentages (Anal. Calcd for $C_{55}H_{79}CoN_3O_2P_3Ti$: C, 65.15; H, 7.85; N, 4.14).

■ ASSOCIATED CONTENT

Supporting Information

The Supporting Information is available free of charge on the ACS Publications website at DOI: 10.1021/acs.organomet.7b00445.

Spectroscopic data (NMR/IR) for complexes **2**−**6** and **8**−**10**; X-ray data collection, solution, and refinement details for **2**, **5**, and **8**−**10**; additional computational details (PDF)

Text file of all computed molecule Cartesian coordinates in a format for convenient visualization (XYZ)

Accession Codes

CCDC 1553733−1553737 contain the supplementary crystallographic data for this paper. These data can be obtained free of charge via www.ccdc.cam.ac.uk/data_request/cif, or by emailing data_request@ccdc.cam.ac.uk, or by contacting The Cambridge Crystallographic Data Centre, 12 Union Road, Cambridge CB2 1EZ, UK; fax: +44 1223 336033.

■ AUTHOR INFORMATION

Corresponding Author

*E-mail: thomasc@brandeis.edu.

ORCID

Diane A. Dickie: 0000-0003-0939-3309
Christine M. Thomas: 0000-0001-5009-0479

Author Contributions

‡These two authors contributed equally.

Notes

The authors declare no competing financial interest.

■ ACKNOWLEDGMENTS

This material is based upon work supported by the U.S. Department of Energy, Office of Science, Office of Basic Energy Sciences, Chemical Sciences, Geosciences, and Biosciences Division, under Award Number DE-SC0014151. Funding for S.L.M. was provided by the Camille and Henry Dreyfus Postdoctoral Program in Environmental Chemistry. We are also grateful for access to the Brandeis University high-performance computing cluster.

■ REFERENCES

(1) (a) Wheatley, N.; Kalck, P. *Chem. Rev.* **1999**, *99*, 3379−3420. (b) Stephan, D. W. *Coord. Chem. Rev.* **1989**, *95*, 41−107. (c) Thomas, C. M. *Comments Inorg. Chem.* **2011**, *32*, 14−38. (d) Gade, L. H. *Angew. Chem., Int. Ed.* **2000**, *39*, 2658−2678. (e) Cooper, B. G.; Napoline, J. W.; Thomas, C. M. *Catal. Rev.: Sci. Eng.* **2012**, *54*, 1−40. (f) Powers, I. G.; Uyeda, C. *ACS Catal.* **2017**, *7*, 936−958.

(2) (a) Hostetler, M. J.; Bergman, R. G. *J. Am. Chem. Soc.* **1990**, *112*, 8621−8623. (b) Hostetler, M. J.; Butts, M. D.; Bergman, R. G. *J. Am. Chem. Soc.* **1993**, *115*, 2743−2752. (c) Hostetler, M. J.; Butts, M. D.; Bergman, R. G. *Organometallics* **1993**, *12*, 65−75. (d) Zhang, Y.; Roberts, S. P.; Bergman, R. G.; Ess, D. H. *ACS Catal.* **2015**, *5*, 1840−1849.

(3) (a) Hanna, T. A.; Baranger, A. M.; Bergman, R. G. *J. Am. Chem. Soc.* **1995**, *117*, 11363−11364. (b) Ferguson, G. S.; Wolczanski, P. T. *J. Am. Chem. Soc.* **1986**, *108*, 8293−8295. (c) Ferguson, G. S.; Wolczanski, P. T.; Parkanyi, L.; Zonnevylle, M. C. *Organometallics* **1988**, *7*, 1967−1979.

(4) Baranger, A. M.; Bergman, R. G. *J. Am. Chem. Soc.* **1994**, *116*, 3822−3835.

(5) (a) Tsutsumi, H.; Sunada, Y.; Shiota, Y.; Yoshizawa, K.; Nagashima, H. *Organometallics* **2009**, *28*, 1988−1991. (b) Walker, W. K.; Anderson, D. L.; Stokes, R. W.; Smith, S. J.; Michaelis, D. J. *Org. Lett.* **2015**, *17*, 752−755. (c) Walker, W. K.; Kay, B. M.; Michaelis, S. A.; Anderson, D. L.; Smith, S. J.; Ess, D. H.; Michaelis, D. J. *J. Am. Chem. Soc.* **2015**, *137*, 7371−7378.

(6) Talley, M. R.; Stokes, R. W.; Walker, W. K.; Michaelis, D. J. *Dalton Trans.* **2016**, *45*, 9770−9773.

(7) (a) Ephritikhine, M. *Chem. Commun.* **1998**, 2549−2554. (b) Fürstner, A. *Chem. - Eur. J.* **1998**, *4*, 567−570. (c) Fürstner, A.; Bogdanović, B. *Angew. Chem., Int. Ed. Engl.* **1996**, *35*, 2442−2469.

(8) (a) James, O. O.; Chowdhury, B.; Mesubi, M. A.; Maity, S. *RSC Adv.* **2012**, *2*, 7347−7366. (b) Corral Valero, M.; Raybaud, P. *Catal. Lett.* **2013**, *143*, 1−17. (c) Cheng, J.; Hu, P.; Ellis, P.; French, S.; Kelly, G.; Lok, C. M. *Top. Catal.* **2010**, *53*, 326−337.

(9) (a) Alonso, D. M.; Wettstein, S. G.; Dumesic, J. A. *Chem. Soc. Rev.* **2012**, *41*, 8075−8098. (b) Sankar, M.; Dimitratos, N.; Miedziak, P. J.; Wells, P. P.; Kiely, C. J.; Hutchings, G. J. *Chem. Soc. Rev.* **2012**, *41*, 8099−8139.

(10) Krogman, J. P.; Thomas, C. M. *Chem. Commun.* **2014**, *50*, 5115−5127.

(11) Krogman, J. P.; Foxman, B. M.; Thomas, C. M. *J. Am. Chem. Soc.* **2011**, *133*, 14582−14585.

(12) Marquard, S. L.; Bezpalko, M. W.; Foxman, B. M.; Thomas, C. M. *J. Am. Chem. Soc.* **2013**, *135*, 6018−6021.

(13) Marquard, S. L.; Bezpalko, M. W.; Foxman, B. M.; Thomas, C. M. *Organometallics* **2014**, *33*, 2071−2079.

(14) Wu, B.; Bezpalko, M. W.; Foxman, B. M.; Thomas, C. M. *Chem. Sci.* **2015**, *6*, 2044−2049.

(15) Zhou, W.; Marquard, S. L.; Bezpalko, M. W.; Foxman, B. M.; Thomas, C. M. *Organometallics* **2013**, *32*, 1766−1772.

(16) An open shell singlet state, $\mathbf{2}^{OSS}$, was also computed and was found to be within 1 kcal/mol of $\mathbf{2}^{S}$ and $\mathbf{2}^{T}$. The optimized geometry, however, is not consistent with the solid-state structure of **2**. While we

can not rule out the participation of a singlet diradical in the equilibrium process, we do not have any concrete evidence for its existence. The similarity in energy of $\mathbf{2}^{S}$, $\mathbf{2}^{T}$, and $\mathbf{2}^{OSS}$ suggests that multiconfigurational computational methods may be more appropriate than DFT for this system.

(17) Greenwood, B. P.; Rowe, G. T.; Chen, C.-H.; Foxman, B. M.; Thomas, C. M. *J. Am. Chem. Soc.* **2010**, *132*, 44−45.

(18) Napoline, J. W.; Krogman, J. P.; Shi, R.; Kuppuswamy, S.; Bezpalko, M. W.; Foxman, B. M.; Thomas, C. M. *Eur. J. Inorg. Chem.* **2013**, *2013*, 3874−3882.

(19) Zilverentant, C. L.; van Albada, G. A.; Bousseksou, A.; Haasnoot, J. G.; Reedijk, J. *Inorg. Chim. Acta* **2000**, *303*, 287−290.

(20) Wu, B.; Gramigna, K. M.; Bezpalko, M. W.; Foxman, B. M.; Thomas, C. M. *Inorg. Chem.* **2015**, *54*, 10909−10917.

(21) The concentration of N_2 in solution is assumed to be sufficiently greater than that of **9** and **10**, such that changes in N_2 concentration in solution over time do not have a large effect on the estimated thermodynamic parameters.

(22) (a) Mindiola, D. J.; Waterman, R.; Jenkins, D. M.; Hillhouse, G. L. *Inorg. Chim. Acta* **2003**, *345*, 299−308. (b) Saes, B. W. H.; Verhoeven, D. G. A.; Lutz, M.; Klein Gebbink, R. J. M.; Moret, M.-E. *Organometallics* **2015**, *34*, 2710−2713.

(23) (a) Mindiola, D. J.; Cummins, C. C. *Organometallics* **2001**, *20*, 3626−3628. (b) Görls, H.; Scholz, J. *J. Organomet. Chem.* **2001**, *626*, 168−170. (c) Hill, J. E.; Fanwick, P. E.; Rothwell, I. P. *Organometallics* **1992**, *11*, 1771−1773. (d) Peulecke, N.; Ohff, A.; Tillack, A.; Baumann, W.; Kempe, R.; Burlakov, V. V.; Rosenthal, U. *Organometallics* **1996**, *15*, 1340−1344. (e) Erker, G.; Dorf, U.; Czisch, P.; Peterson, J. L. *Organometallics* **1986**, *5*, 668−676. (f) Blaschke, U.; Erker, G.; Nissinen, M.; Wegelius, E.; Fröhlich, R. *Organometallics* **1999**, *18*, 1224−1234. (g) Li, L.; Kristian, K. E.; Han, A.; Norton, J. R.; Sattler, W. *Organometallics* **2012**, *31*, 8218−8224.

(24) Cotton, F. A.; Murillo, C. A.; Walton, R. A. *Multiple Bonds Between Metal Atoms*; Springer Science and Business Media, Inc.: New York, 2005.

(25) Pauling, L. *The Nature of the Chemical Bond*, 3rd ed. ed.; Cornell University Press: Ithaca, NY, 1960.

(26) (a) Evans, D. F. *J. Chem. Soc.* **1959**, 2003−2005. (b) Sur, S. K. *J. Magn. Reson.* **1989**, *82*, 169−173.

(27) *APEX2*; Bruker AXS Inc.: Madison, WI, 2012.

(28) Frisch, M. J.; Trucks, G. W.; Schlegel, H. B.; Scuseria, G. E.; Robb, M. A.; Cheeseman, J. R.; Scalmani, G.; Barone, V.; Mennucci, B.; Petersson, G. A.; Nakatsuji, H.; Caricato, M.; Li, X.; Hratchian, H. P.; Izmaylov, A. F.; Bloino, J.; Zheng, G.; Sonnenberg, J. L.; Hada, M.; Ehara, M.; Toyota, K.; Fukuda, R.; Hasegawa, J.; Ishida, M.; Nakajima, T.; Honda, Y.; Kitao, O.; Nakai, H.; Vreven, T.; Montgomery, J. A., Jr.; Peralta, J. E.; Ogliaro, F.; Bearpark, M.; Heyd, J. J.; Brothers, E.; Kudin, K. N.; Staroverov, V. N.; Kobayashi, R.; Normand, J.; Raghavachari, K.; Rendell, A.; Burant, J. C.; Iyengar, S. S.; Tomasi, J.; Cossi, M.; Rega, N.; Millam, J. M.; Klene, M.; Knox, J. E.; Cross, J. B.; Bakken, V.; Adamo, C.; Jaramillo, J.; Gomperts, R.; Stratmann, R. E.; Yazyev, O.; Austin, A. J.; Cammi, R.; Pomelli, C.; Ochterski, J. W.; Martin, R. L.; Morokuma, K.; Zakrzewski, V. G.; Voth, G. A.; Salvador, P.; Dannenberg, J. J.; Dapprich, S.; Daniels, A. D.; Farkas, O.; Foresman, J. B.; Ortiz, J. V.; Cioslowski, J.; Fox, D. J. *Gaussian 09*, revision A.2; Gaussian, Inc.: Wallingford, CT, 2009.

(29) Becke, A. D. *Phys. Rev. A: At., Mol., Opt. Phys.* **1988**, *38*, 3098−3100.

(30) Perdew, J. P. *Phys. Rev. B: Condens. Matter Mater. Phys.* **1986**, *33*, 8822−8824.

(31) (a) Hay, P. J.; Wadt, W. R. *J. Chem. Phys.* **1985**, *82*, 299−310. (b) Hay, P. J.; Wadt, W. R. *J. Chem. Phys.* **1985**, *82*, 270−283. (c) Wadt, W. R.; Hay, P. J. *J. Chem. Phys.* **1985**, *82*, 284−298. (d) Roy, L. E.; Hay, P. J.; Martin, R. L. *J. Chem. Theory Comput.* **2008**, *4*, 1029−1031. (e) Ehlers, A. W.; Bohme, M.; Dapprich, S.; Gobbi, A.; Hollwarth, A.; Jonas, V.; Kohler, K. F.; Stegmann, R.; Veldkamp, A.; Frenking, G. *Chem. Phys. Lett.* **1993**, *208*, 111−114.

(32) Dunning, T. H.; Hay, P. J. In *Methods of Electronic Structure theory*; Modern Theoretical Chemistry series, Vol. 3; Shaefer, H. F., III, Ed.; Plenum: New York, 1976.

(33) (a) Greenwood, B. P.; Forman, S. I.; Rowe, G. T.; Chen, C.-H.; Foxman, B. M.; Thomas, C. M. *Inorg. Chem.* **2009**, *48*, 6251−6260. (b) Krogman, J. P.; Gallagher, J. R.; Zhang, G.; Hock, A. S.; Miller, J. T.; Thomas, C. M. *Dalton Trans.* **2014**, *43*, 13852−13857.